Operational amplifiers circuits for magnetic sensing using perpendicular low coercivity nanoscale spin transfer torque magnetic tunnel junctions

Hugo Nicolas, Ricardo Sousa, Ariam Mora-Hernández, Ioan-Lucian Prejbeanu, Luc Hebrard, Jean-Baptiste Kammerer, Joris Pascal

Operational Amplifiers Circuits for Magnetic Sensing Using Perpendicular Low Coercivity Nanoscale Spin Transfer Torque Magnetic Tunnel Junctions

Hugo Nicolas, *Graduate Student Member, IEEE*, Ricardo C. Sousa, Ariam Mora-Hernández, Ioan-Lucian Prejbeanu, *Senior Member, IEEE*, Luc Hebrard, *Member, IEEE*, Jean-Baptiste Kammerer, and Joris Pascal, *Member, IEEE*

***Abstract*—This paper presents the use of nanoscale perpendicular spin transfer torque magnetic tunnel junctions as magnetic sensing units in which the conditioning electronics consists of simple circuits based on operational amplifiers. This approach allows low power (µW), nanoscale (50 to 100 nm) and high-frequency (100 kHz to 1000 kHz) magnetic measurements, with, in addition, presenting CMOS compatibility for future mass production. Noises levels as low as 2 µT/√Hz are achieved over a dynamic range of up to tens of mT. The different circuits are demonstrated through theoretical modelling and confirmed with experimental measurements on fabricated devices, validating the working principle with sensing elements among the smallest ever reported to our knowledge. Further improvements are however required, in both the proposed electronics and stacks of the junctions, to lower the noise and reach the sub-µT noise level. Hence, this technology could open the way to new metrological possibilities, unaddressed with existing technologies, including photolithographic mask alignment or high-frequency current measurements, in the case of industrial applications, as well as measurements of magnetic beads and ferromagnetic particles detection in life sciences.**

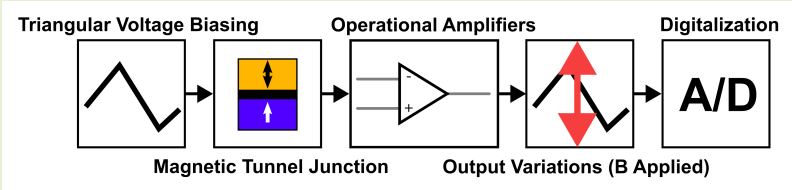

***Index Terms*—Magnetic sensor, magnetic tunnel junction, signal processing electronics, low coercivity, spin transfer torque, STT-MTJ, nanometer scale**

I. Introduction

MAGNETIC sensors are nowadays routinely used in many domains. Over the past decades, many different types of sensors have been developed, based on many different principles, and each of them present different characteristics that allow users to choose among a vast variety of devices depending on the application's needs.

At the top of the list, one can find the extremely popular types, dominated by Hall effect sensors and magnetoresistive sensors (MR) in the category of integrated sensors. On the other hand, one can find Fluxgate sensors, recent optically pumped magnetometers (OPM), diamond nitrogen-vacancy center (NV) magnetometers and well-known SQUIDs (superconducting quantum interference devices) sensors for extremely high resolution measurements sensors (fT) (Fig. 1). In addition to the resolution, cost, sensing element dimensions, temperature operating range, mass production compatibility, or usability are also among the other parameters that the user must evaluate when selecting the correct technology for the application. However, some requirements or combinations of requirements are sometimes difficult to address, for example very high sensitivity (i.e., very low noise), or very high dynamic range, which are only achieved through a limited number of technologies. In the worst cases, no technology is available fulfilling the expected requirements. This includes, for instance,

Manuscript received XXXXXXX XX, XXXX; accepted XXXXXXX XX, XXXX. Date of publication XXXXXXXX XX, XXXX; date of current version XXXXXXX XX, XXXX. This work was funded by the Swiss Nanoscience Institute (No. A18.6) and was partially supported by the European Research Council via grant reference ERC-2022-PoC2 (NANOSENSE No. 101100599) and the National Research Agency in the frame of France 2030 via grant reference ANR-22-EXSP-0006 ADAGE.

Hugo Nicolas and Joris Pascal are with the School of Life Sciences (HLS), University of Applied Sciences, 4132 Muttenz, Switzerland (e-mail: hugo.nicolas@fhnw.ch; joris.pascal@fhnw.ch).

Luc Hebrard and Jean-Baptiste Kammerer are with the laboratory ICube, University of Strasbourg, 67000 Strasbourg, France (e-mail: luc.hebrard@unistra.fr; jb.kammerer@unistra.fr).

Ricardo C. Sousa, Ariam Mora-Hernández and Ioan-Lucian Prejbeanu are with the laboratory Spintec, French Atomic Energy and Alternative Energies Commission (CEA), 38000 Grenoble, France (e-mail: ricardo.sousa@cea.fr; ariam.mora@gmail.com; ioan-lucian.prejbeanu@cea.fr).

Digital Object Identifier XXXXXXXXXXXXXXXXXXXXXXXXXXX

situations where the application requires true punctual measurements, where a lack of available technologies can be observed. This is because most integrated Hall effect sensors require large enough dimensions to obtain a significant deviation of current lines, whereas MR sensors usually exhibit a larger noise at low dimensions.

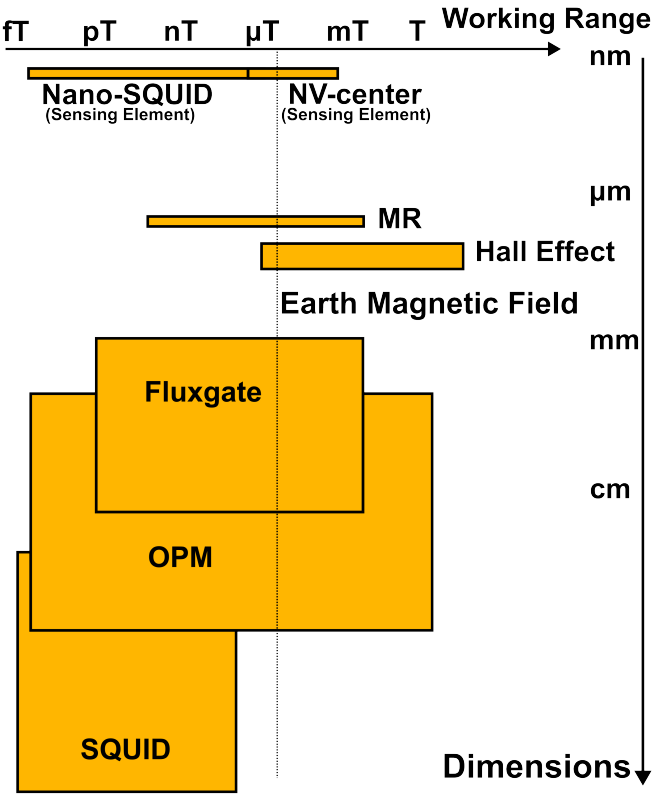

Fig. 1. Typical technologies of magnetic sensors with their associated dimensions. In the case of nano-SQUID sensors and NV-centre sensors, the sensing element can be very small (nm), but the electronics required to operate these sensors is significantly larger and more complex than any circuits used for MR or Hall effect sensors. In addition, most SQUIDs sensors requires very low cooling temperatures, while NV-centre require optical elements making the entire sensing systems relatively large (> mm).

Hence, in this paper, we present the use of simple operational amplifier-based circuits (OpAmp), that allows the use of newly developed custom nanoscale devices, based on perpendicular spin transfer torque magnetic tunnel junctions (STT-MTJs), originally designed for magnetic memories (MRAMs), to be operated as sensing units in a completely unique way.

In section II, the sensing principle and fabricated sensing elements are described. In section III, the proposed architectures of the reading electronics based on operational amplifiers are demonstrated through theoretical and experimental analysis. Finally, section IV discusses the achieved performance and remaining drawbacks of the proposed sensor principles.

II. Sensor Fundamentals

A. Magnetic Tunnel Junction

The MTJs used in this work are perpendicular shape anisotropy MTJs (pMTJs), fabricated as nano-pillar of cylindrical shape with nominal diameter ranging between 50 to 100 nm (50, 80 and 100 nm).

Two different stacks have been evaluated which only differs by the thickness of two specific layers, but all MTJs fabricated are based on a standard MgO barrier with a free and pinned layer (FL and PL respectively) made of $FeCo_8B_{20}$, each layer being 1 to 2 nm thick. Synthetic antiferromagnets (SAF), based on Pt/Co multilayer configuration, are used to pin the magnetization of the PL along the perpendicular axis of the devices. The MgO barrier is made by natural oxidation of 0.75 nm of Mg at a pressure of 0.03 mbar for 10 seconds. The wafers, fabricated with MRAM-compatible (magnetic random-access memories) fabrication processes, were annealed at 300 to 350 °C for 10 minutes. Such an annealing is necessary to enhance the crystalline structure of the FeCoB/MgO/FeCoB and obtain a proper TMR (tunnel magnetoresistance) effect. However, this also demonstrates the capabilities of MTJs to withstand large temperatures, required in CMOS production for back-end-of-line (BEOL) processes (typically limited to around 400 °C). Since the annealing temperatures of front-end-of-line (FEOL) CMOS processes are much higher (typically > 700 °C), MTJs can be safely integrated into CMOS chips during BEOL steps, as in existing commercial MRAM products. To assess the effect of layers' thickness on the MTJs, the wafers were fabricated with wedges (i.e., thickness gradients), allowing for an efficient screening of MTJ properties along the wafer. However, this also results in larger variations in sensing element performance, as seen in Fig. 2. This is also amplified as the fabrication processes remain experimental, resulting in additional possible variations between devices. However, in the case of homogenous wafers with controlled industrial fabrication techniques and equipment, variations can be expected to be significantly reduced, as in existing MTJ-based commercial products (TMR sensors or MRAMs). Hence, further studies are necessary to assess the possible variations achievable in such ideal conditions.

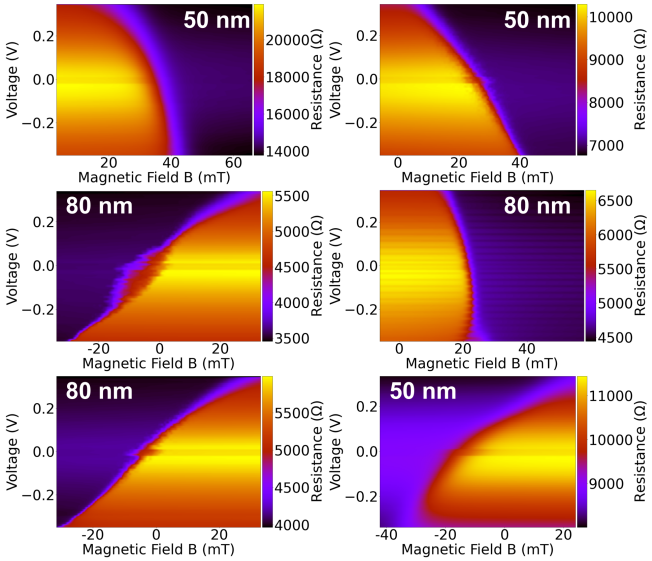

Fig. 2. Phase diagrams of fabricated low coercivity STT-MTJs of different diameters (experimental results). The differences between the MTJs are the results of the wedges as well as experimental fabrication variability.

Although pMTJs are usually fabricated for magnetic memories (MRAMs), the stacks of these MTJs have been designed to exhibit low coercive fields H_c (< 5 mT) and are

dedicated to sensing applications, despite being compatible with standard MRAM fabrication processes. The typical parallel and antiparallel resistance (respectively R_P and R_{AP}) ranges between 1 and 10 kΩ. TMR ratio of 40 to 70 % have been achieved with switching voltages ranging from -400 mV to +400 mV, depending on the external magnetic field. Above these values, devices are subject to breakdown and reliability issues. Offset fields H_0 ranging from -50 to +50 mT have been obtained. Finally, intrinsic sensitivity, measured from the phase diagrams as the slope of the APP/PAP transition region, could reach up to 40 or 50 mV/mT in some measured MTJs (Fig. 2).

B. Spin-Transfer Torque-based Sensing Principle

To operate the fabricated MTJs as magnetic sensing units, a triangular voltage signal is applied across the MTJs to achieve a similar sensing principle as in our previously reported work with high-coercivity MTJs [1], where the switching voltages APP and PAP are proportional to the external magnetic field (Fig. 3). The sensing element used over this paper consists of a unique pMTJ (Fig. 4) combined with the proper electronics.

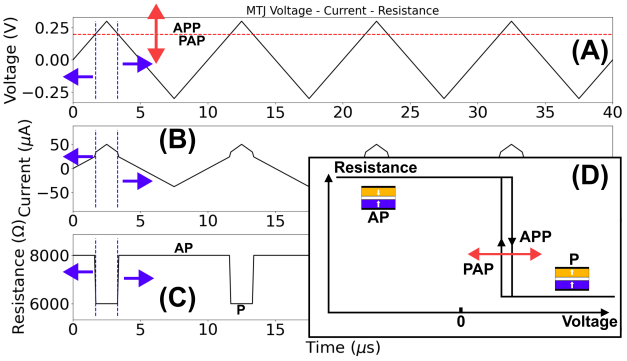

Fig. 3. Low coercivity STT-MTJ-based magnetic sensor measurement principle (simulation). The voltage applied to the MTJ (A), current passing through the MTJ (B), and MTJ resistance (C) are shown. The red arrows indicate how the APP/PAP threshold changes if an external field is applied, while the blue arrows indicate how the signals change with the external field. The inset (D) shows the typical voltage hysteresis cycle of such low coercivity MTJs, with the voltage applied to the MTJ and resistance.

Hence, a periodical reversal between the two states combined with the appropriate electronics, described in the following section III, for threshold or resistance sensing allows for measurements of the magnetic field. To achieve this, a triangular voltage waveform with a peak-to-peak amplitude of ± 350 to ± 400 mV and with typical frequencies of 100 kHz to 1 MHz is applied to the MTJ, while the MTJ is connected to the electronics required to observe the sensing behavior (Fig. 3). Based on perpendicular magnetic anisotropy (PMA), these MTJs exhibit out-of-plane measurements capabilities, as opposed to most TMR sensors, also based on MTJs but exhibiting in-plane measurements capabilities.

C. Experimental Setup

To demonstrate the measurement principles, the MTJs were fabricated on 4" (100 mm) wafers, containing up to 20,000 MTJs with diameters of 50 to 100 nm. The electronics, entirely based on discrete components, were fabricated on custom printed circuit boards (PCBs) and are described in Section III. Three different designs were successfully demonstrated. The MTJs were tested in a setup (Fig. 3) allowing the exposure to fields ranging from -200 to +200 mT with an externally controlled electromagnet, which, despite allowing strong field generation, presents hysteresis due to the flux concentrator used (i.e., hysteresis that needs to be disregarded in the measurements from section III).

To connect the electronics to the MTJ, a custom non-magnetic probe was used. During the typical measurement sequence, the wafer is moved until the MTJ to be tested is placed right below the probe, and the two pads are aligned with the two tips of the probe. At this point, the wafer is moved up, allowing the contact to take place, and connects the two pads to the electronics. The measurements are then performed, and the operation can be repeated for another MTJ, allowing fast and automated measurements.

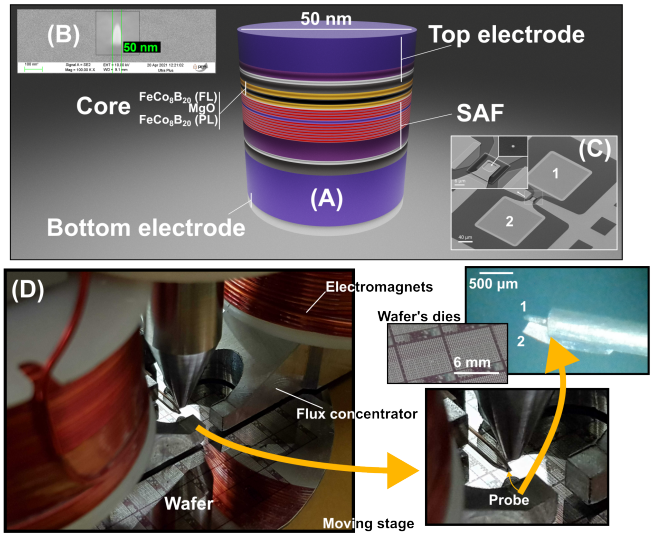

Fig. 4. Experimental setup. The typical 3D model of a pSTT-MTJ pillar is shown (A) with the corresponding SEM (scanning electron microscope) image of a fabricated device (B). This represents the sensing element used in this work. To access the MTJ and connect it to the electronics, the devices are fabricated with two large pads (numbered 1 and 2), connecting the top and bottom electrode to the probe of the test setup, as shown in the SEM image (C). Test setup (D) used to assess the performance of the proposed sensor. The wafer, containing the fabricated MTJs, is placed under the electromagnet and a testing probe is used to access the MTJ and connect the two electrodes to the PCB.

Commercially available OpAmps, i.e., LMV116 (Texas Instrument, USA), were used to create the discrete version of each of the proposed circuits on PCBs. These OpAmps were chosen among many other possible references for their low power idle consumption (0.6 mA), rail-to-rail operation, and high GBW (gain-bandwidth product) of 45 MHz. Such performance are also typically what can be reasonably achieved in future custom integrated circuits and are therefore typical of possible future performance. The open-loop gain of such OpAmp is 85 dB (300e6), making the assumption of ideal OpAmps for establishing the output equation of the system valid. The general noise induced by these OpAmps and electronics are negligible (< 100 nV/√Hz) in comparison to the large noise induced by the stochasticity of the MTJ (typically > μV/√Hz). In addition, the offset of these OpAmps (< 6 mV) is also negligible for this proof-of-concept. Finally, capacitors, Schottky diodes, and resistors were also based on SMD (surface mounted device) components.

The ADC (analog-to-digital converter) used in sections III.A

and III.B is the ADS1259 (Texas Instrument, USA), based on a Sigma-Delta architecture, and offering a resolution of 24 bits (300 nV/LSB), sampled at 2 kHz. This ADC exhibits a power consumption of 13 mW, and was chosen for its small package, internal reference and simplicity of use, even if several other references could also be used for this demonstration. In Section III.C, the ADS8681 (Texas Instrument, USA), based on a successive approximation register architecture (SAR), was chosen among other references for its internal reference, the high frequency capability of up to 1 MHz of sampling rate, with a resolution of 16 bits (78 µV/LSB), at a power consumption of 50 mW.

III. Operational Amplifier Conditioning Circuits

To operate the low coercivity MTJs as magnetic sensors using the STT effect, different conditioning architectures have been tested and are described in the following subsections. The use of these junctions allows for higher sensitivity and better noise performance to be achieved, in comparison to our previously reported work based on high-coercivity MTJs [1].

A. Operational Amplifier Circuit

In the first approach, the MTJ was implemented as a variable resistor within a typical integrator circuit based on a single operational amplifier, as depicted in Fig. 5.

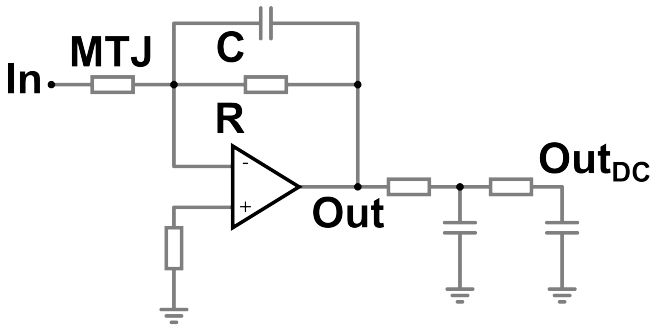

Fig. 5. Initial circuit proposed for the measurements of low coercivity STT-MTJs based on a single operational amplifier.

The MTJ was connected between the input signal, coming from the waveform generator, and the virtual ground of the operational amplifier, ensuring, for proper behavior, that the voltage applied between the two electrodes of the MTJ is always referenced to a constant potential. Hence, the circuit works by integrating the input signal with a gain which is defined by the resistance of the MTJ, R and C. The resistor R and capacitor C were chosen to be respectively 82 kΩ and 1 nF. In this configuration, the integration of any triangular waveform results in a quadratic signal at the output of the amplifier. Since the resistance is constantly alternating between the P and AP states, this creates a variable gain over one period of the input signal. As the MTJ stays in one state longer or shorter than in the other state depending on the magnetic field, this creates an asymmetry in the gain, resulting in an output signal proportional to the magnetic field. In this condition, the dc offset of the quadratic signal is affected by the external magnetic field. Therefore, a simple passive second-order RC (resistor-capacitor) LPF (low-pass filter) with a cut-off frequency of 160 Hz (arbitrarily chosen) is then used to retrieve the dc offset of the signal and output a signal directly proportional to the magnetic field, which is sampled by the ADC.

The output equation of the proposed circuit is given by (1).

$$V_{out}(V_{in}(t),B) = \int \frac{-V_{in}(t)dt}{C.R_{MTJ}(V_{in}(t),B)} + Cst.e^{\frac{-t}{RC}} \quad (1)$$

For theoretical modeling, two approaches were tested. During LTspice simulations, ideal OpAmp models were used, with standard ideal resistors and capacitors. The input voltage of the circuit was pre-generated with Python as a triangular voltage, saved as a text file (voltage with time stamp) and used as a piecewise linear (PWL) generator in LTspice, at the input of the circuit. In parallel, the resistance of the MTJ was also pre-calculated in Python for each voltage data point (from the input voltage file) and set as P or AP states depending on the voltage, in comparison to an arbitrary threshold. This allows the generation of a second text file, which was used in LTspice for a resistor whose value at any time stamp was given by the value in this second file. The rest of the circuit was then simulated by LTspice, and the output voltage of the circuit was saved in a data file and evaluated in Python.

For equation-based modeling, Python was used, and the output voltage of the circuit was calculated using equation (1) at each time step. The MTJ was also implemented as a bi-stable resistor (AP and P states), whose value was determined at each time step by comparing the input voltage with an arbitrary threshold.

Repeating these simulations for different threshold values for the AP/P/AP transitions allows us to generate the output sensitivity of the simulated sensor (Fig. 6).

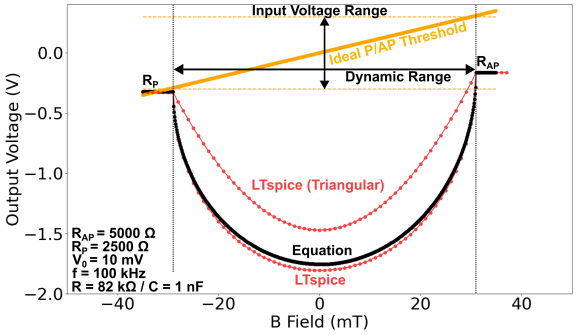

Fig. 6. Integrator-based theoretical output of the proposed circuit, calculated using the proposed equation (1) or LTspice (simulations). The parameters for the simulation are shown for reference, and the switching APP/PAP threshold limits are also visible. The effect from the use of input sine or triangular signals is visible.

The experimental measurements of the MTJs-based magnetic sensor showed a successful working principle (Fig. 7 and Fig. 8). To extract the sensitivity of the sensor, a discrete sweep of the magnetic field was performed. For each point, magnetic field was set at a constant dc level, and the voltage at the output of the LPF was sampled by the same ADC. For each magnetic field step, 8192 data points were sampled, and the median was calculated to obtain the output value of the sensor for each step. The output characteristic of the sensor was obtained and sensitivities of 5 to 15 mV/mT were achieved. The complete magnetic field range where output voltage variations can be observed reaches up to 40 mT (i.e., ± 20 mT around the offset field), depending on the MTJ, always through a typical

'U' shape (Fig. 8). Due to the output characteristics shape, the assessment of the non-linearity is more complicated to define. However, ± 1 to 3 % FS (full scale) can be achieved over up to 10 mT in the most linear region, and more complicated linearization techniques (e.g., lookup table, offset cancellation with feedback coils) could be used for better performance over the entire dynamic range. Noise measurements were also performed. NPSD (noise power spectral density) was typically between 0.1 to 0.3 mV/√Hz, corresponding to 10 to 40 µT/√Hz, with best performance obtained from both sides of the offset field, as low as 2 µT/√Hz depending on the MTJ. The typical rms noise was 1 to 10 mV, corresponding to up to 500 µT over a bandwidth of hundreds of Hz, defined by the cut-off frequency of the LPF (160 Hz in this example). As can be observed in the output of the circuit, a parasitic oscillation (35 MHz) is present. It is induced by a parasitic capacitance interacting with the amplifier causing oscillations. Such parasitic capacitance can be either the intrinsic capacitance of the MTJ (typically 50 to 100 pF) and/or from the SMA cables (typically 50 to 100 pF/m) used. Since all these oscillations are filtered by the output LPF, this does not cause any issues for our proof-of-concept and was not investigated further.

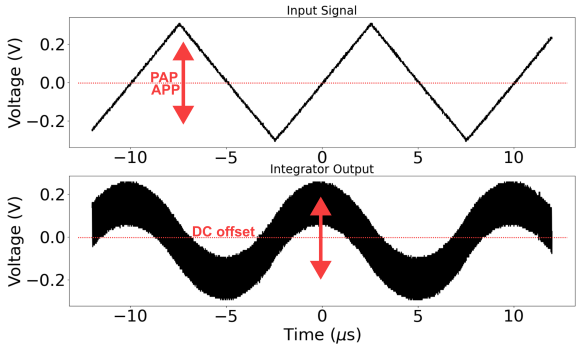

Fig. 7. Input and output signals of the proposed initial circuit (experimental results).

Theoretical (Fig. 6) and experimental (Fig. 8) measurements are in good agreement, validating the working principle of the proposed method.

B. Improved Architecture

As seen in the previous section III.A, the presented initial method demonstrates the working principle with, however, two main issues. The first is a symmetry in the output voltages, making it impossible to differentiate positive or negative magnetic fields centered around the offset. The second observed issue is a dead zone, located around the offset field, where a null sensitivity is observed. Hence, a second approach described in this section aims to overcome these metrological problems. To overcome these drawbacks, the circuit described above can be slightly modified (Fig. 9). In this second approach, the MTJ is placed as the input resistor of an inverting amplifier. In the same condition as in the first method, the gain of the circuit changes over one period, as the MTJ alternates between the P and AP states, and as a result, the output signal corresponds to the input signal amplified with a variable gain proportional to the external magnetic field. However, this does not solve the symmetry problems, as the filtering of this output signal still demonstrates such a symmetry issue. To address the

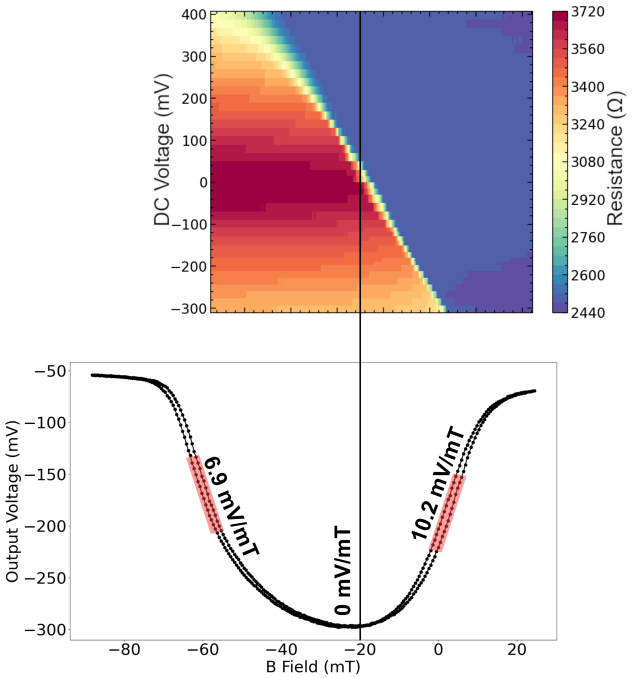

Fig. 8. Achieved performance of the proposed initial circuit for a 80 nm STT-MTJ (experimental results). Typical sections of the curves where the linearities were evaluated are highlighted in red. Outside these regions, the response is non-linear and linearization approaches would be required, and/or optimization of the stack / electronics allowing for enhanced linearity.

issues directly, this signal needs to be injected into a precision OpAmp-based rectifying circuit, whose input signal is fully rectified at the output. The output of the rectifying circuit can then be filtered through a second-order, RC LPF, with a cut-off frequency similar to that in the first method, resulting in a signal proportional to the magnetic field that can be sampled by the ADC. Through such an approach, the average value of the output signal is proportional to the magnetic field and not the dc offset, as in the integrator-based approach. The gain of the proposed circuit is given directly by equation (2), with R chosen to be 8.2 kΩ. This value of R allows different MTJs to be tested without saturating the amplifier.

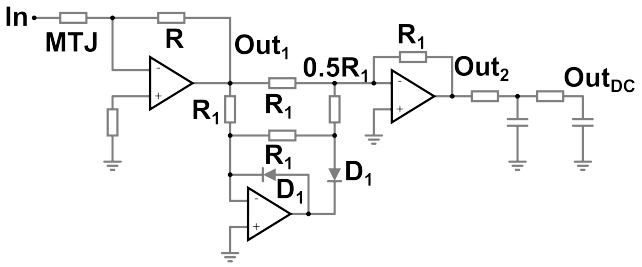

Fig. 9. Improved architecture for the measurement circuit.

The equation giving the output of the circuit is given by (2).

$$V_{out}(V_{in}(t), B) = \left| \frac{-V_{in}(t)R}{R_{MTJ}(V_{in}(t), B)} \right| \quad (2)$$

For the circuit simulation (Fig. 10), the same approach was used for the MTJ modeling, as described in Section III.A (using

the LTspice simulation or using equation (2)). To assess the impact of possible coercivity, the pre-calculation of the resistance of the MTJ in Python was modified by implementing a simple hysteresis threshold. Hence, it can be seen that the use of non-zero coercivity in the MTJ does not appear to have any impact on the non-sensitive region around the offset field.

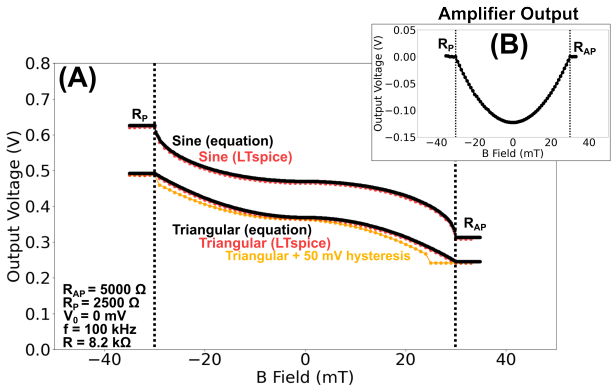

Fig. 10. Rectifier-based theoretical output characteristic (simulations), calculated using the proposed equation (2) or LTspice. The parameters for the simulation are shown for reference. The effect from the use of input sine or triangular signals is visible (A). The direct output of the first amplifier is shown for reference (B).

Experimental measurements were also performed (Fig. 11 and Fig. 12). Sensitivity values of 1 to 5 mV/mT were achieved. NPSD was typically 0.04 to 0.1 mV/√Hz, corresponding to 10 to 40 µT/√Hz, with best performance obtained around the offset field, as low as 2 µT/√Hz depending on the MTJ. The typical rms noise was 0.5 mV, corresponding to 200 to 300 µT over a bandwidth of hundreds of Hz, depending on the cut-off frequency of the LPF, similarly to the previous method (160 Hz). Similarly, parasitic oscillations were observed as the result of the parasitic capacitances of either the MTJ and/or circuit. They remain filtered by the output LPF, and do not cause any issues for our proof-of-concept.

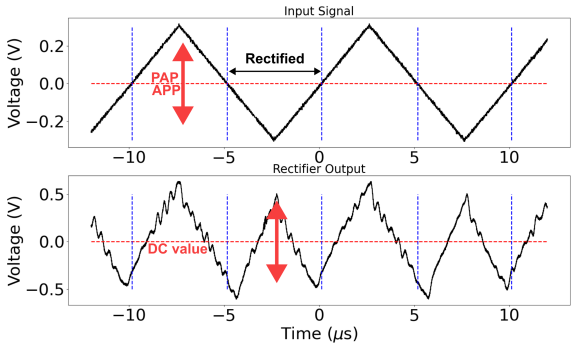

Fig. 11. Input and output signals of the proposed rectifier circuit (experimental results).

Hence, similarly, the theoretical (Fig. 10) and experimental (Fig. 12) measurements agree well, validating the working principle of the proposed second method.

C. High-Frequency Architecture

Finally, one of the big advantages in the use of STT-MTJs as sensing units lies in the capability of high-frequency reversals, which inherits from high-frequency MRAMs operation requirements for high-speed operations (> MHz). To assess

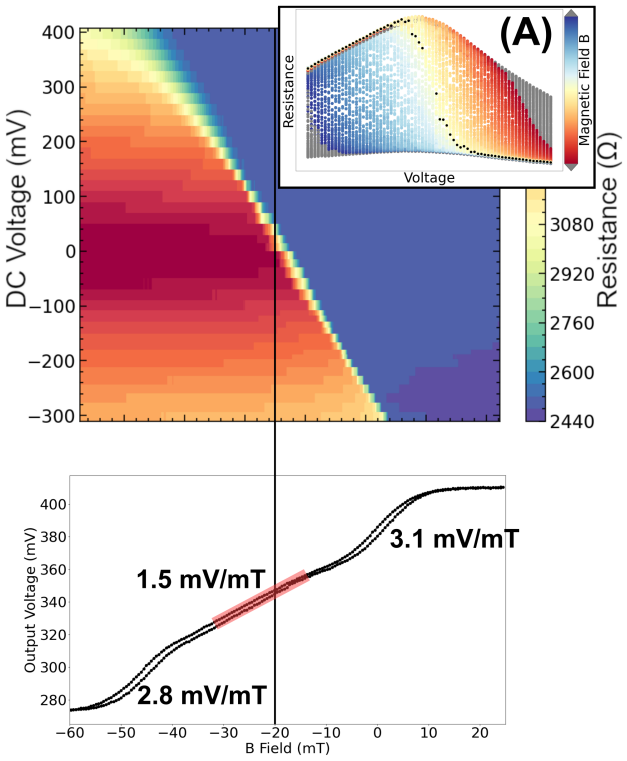

Fig. 12. Achieved performance of the proposed second circuit for a 80 nm STT-MTJ (experimental results). Typical part of the curve where the linearities were evaluated are highlighted in red. In addition, as can be observed, the zero-sensitivity region is absent from the experimental measurements compared to the simulated results. This is a consequence of the low-coercivity MTJs not being true bistable systems, with two well-defined resistance states. Experimentally, the transition between the two limit states has intermediate values that were not taken into account in the simulation. These values can be observed in the hysteresis cycles measured at different bias voltages for different applied external fields (A). This significantly affects the output characteristics around the offset field.

these high-frequency performance in sensing applications, additional measurements were performed on these junctions.

To operate the MTJs at higher frequencies, the circuit needs to be adjusted, to obtain an output voltage which allows synchronous sampling, synchronized with the input signal, removing any aliasing possibility and simplifying the overall circuit. Hence, based on the second circuit described above, simple modifications allow a single-period reversal to be sampled and offer high-bandwidth capability. To achieve this, the second approach demonstrated previously, based on the rectifying circuit, was reused. However, the output voltage obtained at the output of the rectifying circuit needs to be injected directly into a second stage, based on a standard OpAmp integrating circuit, which integrates the resulting signal over the duration of one period of the input signal.

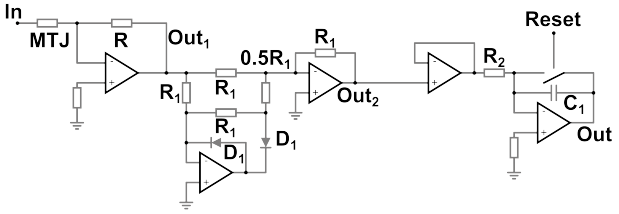

Fig. 13. High-frequency version of the proposed circuit for the measurements of low coercivity STT-MTJs.

To precisely control this integration, a simple reset switch, placed in parallel of the integrating capacitor, is used, allowing for the value of the final output stage to be reset at each new period. For each completion of a period of the input signal, the ADC is configured to sample the value at the output of the integrating circuit, followed by a reset of the circuit, allowing for a new period to be integrated. This corresponds to one measurement cycle, which is then repeated for every new period, allowing high-frequency measurement to be performed. This reset switch is controlled by an external MCU (microcontroller unit), which is also in charge of triggering and reading the ADC. Finally, to detect the periods, a simple comparator was used, comparing the input signal with the ground, allowing a new rising edge for each new period to be produced. This triggers the MCU to perform the reading of the ADC followed by the reset of the circuit. The complete circuit is depicted in Fig. 13 with the control signals shown in Fig. 15. The chosen values are R of 8.2 kΩ, and R_2 and C_1 chosen to have a high cut-off frequency above 50 kHz for a 100 kHz signal, in this case 79 kHz. However, as seen in these figures, such an architecture only allows a sampling at a frequency of half the input frequency (50 kHz in this example), as every other period is used for the reset and conversion. To allow complete sampling at maximum bandwidth, one can simply invert the polarity signal and inject it into a second integrator stage, running in parallel to the first stage, allowing for the sampling of all periods.

The equation giving the output of the sensor is given by (3).

$$V_{out}(V_{in}(t),B) = \frac{-R_2}{C_1}\int_0^T \left|\frac{-V_{in}(t)R}{R_{MTJ}(V_{in}(t),B)}\right| dt \qquad (3)$$

Using LTspice simulation, following the same approaches as described in section III.A for the simulation of the MTJ, the output of the circuit can be simulated (Fig. 14), demonstrating the proper behavior.

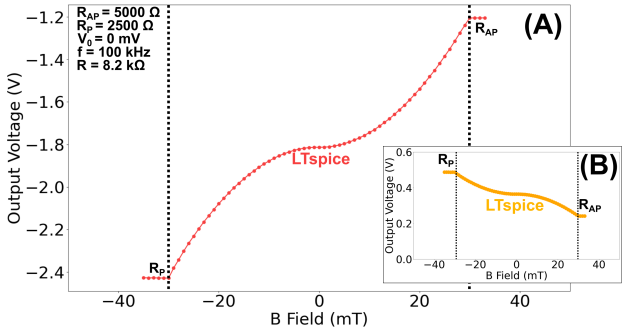

Fig. 14. Output characteristic of the proposed high-frequency circuit (A). The output of the circuit proposed in section III.B is shown for reference (B) (theoretical results).

The measurements of experimental signals as well as simulations demonstrate the working principle of the proposed method, with proper oscillating outputs, and show the dynamic metrological capabilities of the sensor (Fig. 16).

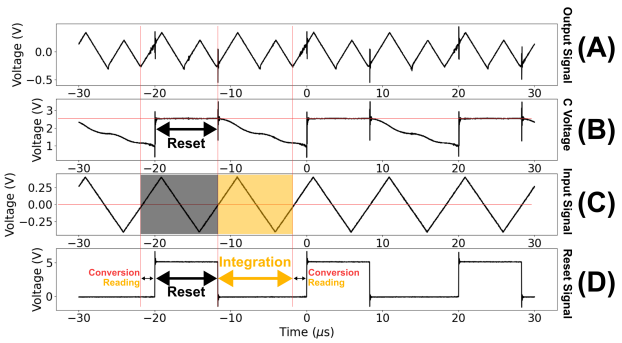

Fig. 15. Main signals of the high-frequency circuit (experimental results). The output voltage of the rectifier (A), capacitor voltage (B), input voltage (C) and reset signal (D) are shown.

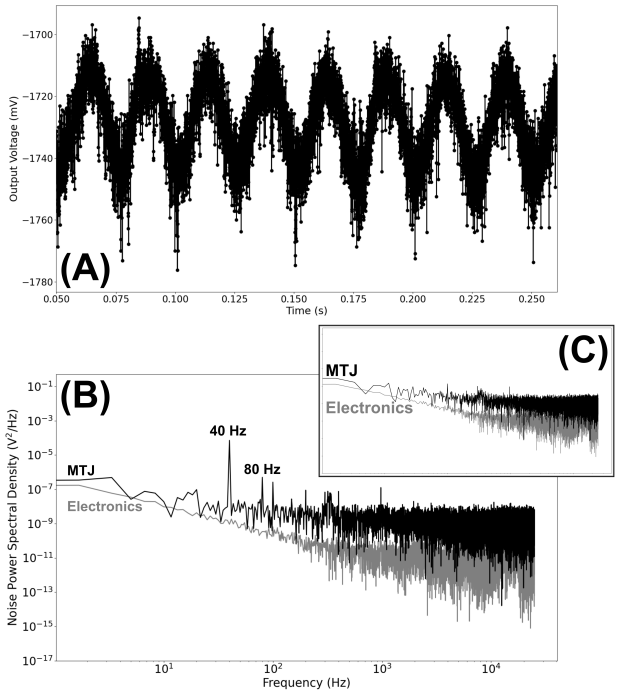

Fig. 16. Measurement of an ac sine wave magnetic field of ± 5 mT at 40 Hz with a 100 nm MTJ (experimental results). The time domain (A) and the frequency domain (B) are shown. The inset (C) shows the NPSD measured in the absence of field. The noise of the electronics, measured by replacing the MTJ with a 5 kΩ resistor is shown in both measurements.

IV. Discussion

A. Low Coercivity STT-MTJ Magnetic Sensor

This paper presents the use of dedicated low coercivity STT-MTJs as sensing units with simple electronic circuits. Simple operational amplifier-based solutions for operating these devices as sensing elements have been successfully proposed and demonstrated through experimental measurements. Three different circuits have been proposed and validated experimentally. The first (Fig. 5) based on a simple integrator allows for easy implementation of the proposed STT-MTJ measurement principle. This leads to very compact measurement systems through a unique operational amplifier.

The second one (Fig. 9), implementing an OpAmp-based precision rectifier, allows for the suppression of the symmetrical output issue by adding a few additional components and two diodes. However, in both cases, because these MTJs exhibit switching voltages crossing 0 V, this creates a reduced sensitivity or even a dead zone, and a complicated situation to solve, as electronics working at very low voltages become highly challenging to design. Hence, if electronics solutions and circuits could eventually be implemented to minimize this effect, the most effective solution would be to shift the entire response of the MTJs to a single polarity, either positive or negative, allowing the switching voltages to remain far from 0 V, at the expense of higher power consumption. However, in-depth studies have not yet been performed on the physical feasibility of such solutions. In any case, it would require significant effort from the design and fabrication of the devices. Finally, another approach (Fig. 13), based on a modified version of these circuits, allows for single-period measurements without adding significant complexity, and maximizes the bandwidth at the expense of a larger rms noise, allowing large bandwidth, of up to several hundreds of kHz (100 kHz with reversals observed up to 1000 kHz), covering more specific applications requiring high-speed measurements. Additional enhancements to the stack are necessary to achieve zero offset fields and to further increase the inherent sensitivity of the MTJs. Finally, dedicated analysis of the stochasticity observed in the reversals will allow for a better understanding of the origin and solutions of such phenomena, allowing for lower noise to be achieved through stack optimization and better control of the MTJs.

B. Advantages and State-of-the-art Comparison

Although many technologies of magnetic sensors exist, only a few of them are available as integrated circuits and represent the typical competitive technologies targeted by the new measurement principle presented. This includes almost exclusively Hall effect, TMR, and AMR (anisotropic MR) sensors, with the exception of a few GMR (giant MR) sensors, MEMS (micro-electromechanical systems) sensors or dedicated proprietary technologies. To assess how the sensing elements presented in this work perform compared to existing sensors, the remainder of this section aims to review existing devices and compare their performance with the results achieved throughout this work. However, among commercial products, sensing elements are often industrial secrets and only a few references with available dimensions can be analyzed. In addition, only a few experimental works have been conducted that focus on the development of nanoscale magnetic sensors, with less than ten research approaches found [3], [4], [5], [6]. This is due to several factors, including technological challenges, applications limitations, cost or physics limitations (e.g., noise vs dimensions relationship in some MR technologies [2]). The different sensors and works found are compared with the proposed STT-MTJ magnetic sensors in Fig. 17. As can be observed, the dimensions of the MTJs used in this work are among the smallest sensitive elements ever reported, with noise performance comparable with nanoscale TMR experimental devices. In addition, since the presented sensing principle is similar to the fluxgate technique (i.e., periodical reversals of a ferromagnetic layer with a threshold depending on the magnetic field), one can also compare the performance achieved with existing fluxgate sensors, as shown in Fig. 17, where NPSD, current and sensing volume are compared, in addition to a comparison factor known as the figure of merit (FoM) and calculated as $(N.I.V^{1/3})^{-1}$, with N the NPSD, V the volume of the sensing element and I the polarization current. This demonstrates that the presented technology based on STT-MTJs is showing good performance in comparison to existing technologies when the size is considered, following the same linear trend, which, in the case of standard fluxgate, is most likely linked to the Barkhausen noise, representing the noise limits.

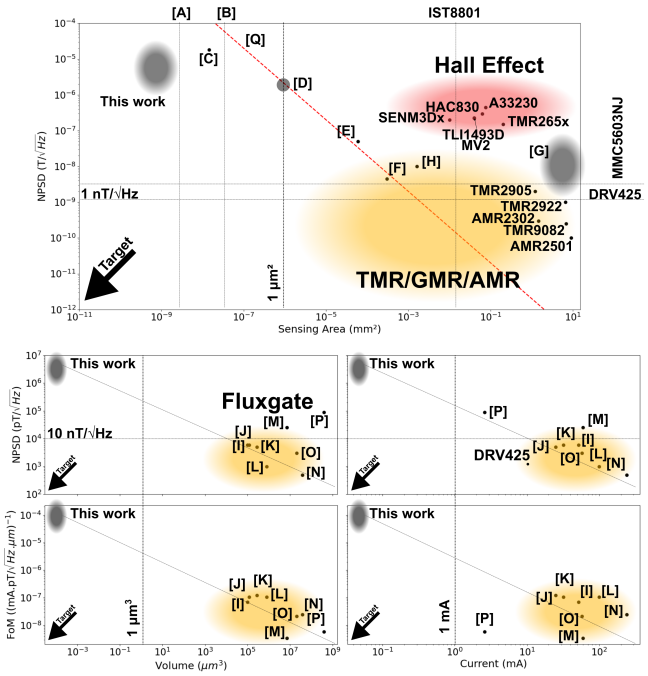

Fig. 17. Comparison of existing technologies with the presented STT-MTJs sensors approaches (A: [3], B: [4], C: [5], D: [6], E: [7], F: [8], G: [9], H: [10]) and (I: [11], J: [12], K: [13], L: [14], M: [15], N: [16], O: [17], P: [18]). The red dashed line (Q: [19]) represent the noise of a TMR sensor based on a single MTJ as a function of its area.

However, the dimensions of the sensors and the noise power spectral density are not the only parameters that are important in magnetic sensors. Hence, among other parameters, one can also look at the following ones.

This includes CMOS compatibility, as MTJs for MRAM cells are or will become natively compatible with mass production processes with the development of this technology.

This sensor also exhibits a large dynamic range of up to tens of mT, higher than most MR sensors, with, depending on the region chosen, a linearity in the same order of magnitude than MR sensors, with ± 1 to 5 % FS (full scale), making the presented sensing principle also competitive in this domain even without the use of linearization techniques (lookup table, feedback coil, etc.).

Furthermore, integrated Hall effect and MR sensors typically consume 1 to 5 mA at a voltage of 1.8 to 5 V (typically standard values of 1.8, 2.5, 3.3 or 5 V), powering either the entire analog and digital circuits (e.g., ADC and/or digital communication with a MCU) or only the sensing

element (in the case of analog output devices). However, such current consumption values can be much higher, for instance in the case of higher polarization or spinning current architecture in Hall effect sensors (10 to 25 mA), or in the case of set-reset operation in AMR sensors (up to few A for short duration). In addition, since these sensors are based on variations in resistance of a physical device, higher resistances also come with stronger thermal noise ($\propto 4k_BTR$, with k_B the Boltzmann constant, T the temperature and R the resistance of the element) and are therefore often avoided, leading to stronger current consumption. On the other hand, the presented STT-MTJ magnetic sensor is currently based on discrete components, hence, power consumption is difficult to fairly compare. However, the entire PCBs used over this work typically consume 5 to 10 mA, with up to 90 to 95 % being used by the ADC only. The MTJ (sensitive element) itself typically consumes less than 200 µA at a voltage of 0.3 to 0.4 V (resulting in a power dissipation as low as 10 µW), depending on the diameter of the MTJ, making the presented method very low power in comparison to existing technologies such as low power TMR sensors.

One can also observe that Hall effect sensors are nowadays available with three sensing axis (X, Y or Z) possibilities. However, GMR and TMR sensors are very frequently available as only sensitive to the plane of the wafer (X or Y), due to technical challenges and difficulties for Z-axis sensing. On the other hand, the presented STT-MTJ sensor is sensitive to the perpendicular plane of the wafer (Z), making it complementary to existing MR technologies.

Moreover, while Hall effect sensors can be virtually exposed to unlimited magnetic field without any damage, AMR sensors are requiring a set-reset functionality to be exposed to stronger fields, and the absence of such architecture greatly reduces the maximum possible field exposure without affecting the performance of the device. TMR and GMR sensors are often based on a PL (through a different mechanism), and the maximum field exposure can be significantly high depending on the H_c of the PL or the design of the SAF (synthetic antiferromagnet). Hence, the presented STT-MTJ falls into this last category, allowing it to withstand strong field exposure, of up to ± 200 mT without any damage.

Finally, the presented measurement principle based on the reversals of resistive states allows for high-frequency measurements to be performed, since MTJs for MRAMs cells are intrinsically low capacitance (nF to pF) and offer high-speed compatibility with nanoseconds reversals. Hence, using such properties associated with the proper electronics, a bandwidth of up to 1 MHz has been achieved. Existing technologies usually exhibit some limitations, such as induced by the RC constant of the sensing elements. In the case of Hall effect sensors, the use of the spinning current, used to enhance the performance of the sensor is also among limitations in the maximum frequency achievable due to technical difficulties of the electronics (cost, size, etc.). This makes the presented technology competitive for high-speed measurements at low noise, often poorly addressed by existing standard technologies. This is because the use of multiple (for synchronous averaging), high-speed nanoscale sensing elements allows both issues (noise and bandwidth) to be addressed at the same time. However, further studies are also necessary to assess the impact of the different diameters on the performance of the sensor, mainly in terms of noise.

V. Conclusion

In this paper, we successfully demonstrated the use of low coercivity, perpendicular nanoscale MTJs operated with simple operational amplifier circuits, which allows the STT effect to be used to create magnetic sensing units from these junctions. The proposed circuits and fabricated MTJs offer CMOS compatibility for future monolithic integration or mass production. In this paper, MTJs, presenting nominal diameters as small as 50 nm up to 100 nm, have been experimentally demonstrated. This represents to our knowledge the smallest sensing elements ever reported, with achieved performance (including bandwidth or power consumption) which are outperforming existing nanoscale sensors at room temperature and low cost. Further assessment of the physics of the low coercivity MTJs as well as improvements in the electronics will eventually allow sub-microtesla resolution, opening the way to new metrological possibilities.

References

[1] H. Nicolas, R. C. Sousa, A. Mora-Hernández, I.-L. Prejbeanu, L. Hebrard, J.-B. Kammerer, and J. Pascal, “Conditioning Circuits for Nanoscale Perpendicular Spin Transfer Torque Magnetic Tunnel Junctions as Magnetic Sensors,” IEEE Sensors Journal, vol. 23, no. 6, pp. 5670-5680, March 2023, 10.1109/JSEN.2023.3241967.

[2] Z. Q. Lei, G. J. Li, W. F. Egelhoff, P. T. Lai, and P. W. T. Pong, “Review of Noise Sources in Magnetic Tunnel Junction Sensors,” IEEE Transactions on Magnetics, vol. 47, no. 3, pp. 602-612, March 2011, 10.1109/TMAG.2010.2100814.

[3] Z. M. Zeng, P. Khalili Amiri, J. A. Katine, J. Langer, K. L. Wang, and H. W. Jiang, “Nanoscale magnetic tunnel junction sensors with perpendicular anisotropy sensing layer,” Applied Physics Letters, 101(6):062412, August 2012, 10.1063/1.4744914.

[4] C. Albon, A. Weddemann, A. Auge, K. Rott, and A. Hutten, “Tunneling magnetoresistance sensors for high resolutive particle detection,” Applied Physics Letters, 95(2):023101, July 2009, 10.1063/1.3179241.

[5] D. C. Leitao, E. Paz, A. V. Silva, A. Moskaltsova, S. Knudde, F. L. Deepak, R. Ferreira, S. Cardoso, and P. P. Freitas, “Nanoscale Magnetic Tunnel Junction Sensing Devices With Soft Pinned Sensing Layer and Low Aspect Ratio,” IEEE Transactions on Magnetics, 50(11):1–8, November 2014, 10.1109/TMAG.2014.2320606.

[6] E. Monteblanco, A. Solignac, C. Chopin, J. Moulin, P. Belliot, N. Belin, P. Campiglio, C. Fermon, and M. Pannetier-Lecoeur, “Constant TMR magnetic field sensor detectivity with bias voltage,” arXiv:2103.04750.

[7] J. Amaral, J. Gaspar, V. Pinto, T. Costa, N. Sousa, S. Cardoso, and P. Freitas, “Measuring brain activity with magnetoresistive sensors integrated in micromachined probe needles,” Applied Physics A, 111(2):407–412, May 2013, 10.1007/s00339-013-7621-7.

[8] L. Huang, Z. H. Yuan, B. S. Tao, C. H. Wan, P. Guo, Q. T. Zhang, L. Yin, J. F. Feng, T. Nakano, H. Naganuma, H. F. Liu, Y. Yan, and X. F. Han, “Noise suppression and sensitivity manipulation of magnetic tunnel junction sensors with soft magnetic Co70.5Fe4.5Si15B10 layer,” Journal of Applied Physics, 122(11), September 2017, 10.1063/1.4990478.

[9] J. E. Davies, J. D. Watts, J. Novotny, D. Huang, and P. G. Eames, “Magnetoresistive sensor detectivity: A comparative analysis,” Applied Physics Letters, 118(6):062401, February 2021, 10.1063/5.0038187.

[10] C. Chopin, J. Torrejon, A. Solignac, C. Fermon, P. Jendritza, P. Fries, and M. Pannetier-Lecoeur, “Magnetoresistive Sensor in Two-Dimension on a 25 um Thick Silicon Substrate for In Vivo Neuronal Measurements,” ACS Sensors, 5(11):3493–3500, November 2020, 10.1021/acssensors.0c01578.

[11] M. Schneider, S. Kawahito, Y. Tadokoro, and H. Baltes, “High sensitivity CMOS microfluxgate sensor,” International Electron Devices Meeting. IEDM Technical Digest, pp. 907–910, December 1997, 10.1109/IEDM.1997.650528.

[12] S. Kawahito, C. Maier, M. Schneiher, M. Zimmermann, and H. Baltes, “A 2D CMOS microfluxgate sensor system for digital detection of weak

magnetic fields," IEEE Journal of Solid-State Circuits, 34(12):1843–1851, December 1999, 10.1109/4.808909.
[13] T. Jager, M. Audoin, M. Beranger, R. Cuchet, E. Delevoye, B. Guihlamat, and R. Hida, "Microfluxgate Sensors for High Frequency and Low Power Applications," TRANSDUCERS2007 - 2007 International Solid-State Sensors, Actuators and Microsystems Conference, pp. 2585–2588, June 2007, 10.1109/SENSOR.2007.4300700.
[14] H. Joisten, B. Guilhamat, M. Audoin, J.-M. Leger, R. Cuchet, G. Barrois, J.-B. Albertini, P. Gaud, P. Renaux, D. Bloch, and B. Viala, "Microfluxgate performance improvement in microtechnology," IEEE Transactions on Magnetics, November 2005, 10.1109/TMAG.2005.854794.
[15] C.-C. Lu, Y.-C. Lin, Y.-Z. Tian, and J.-T. Jeng, "Hybrid Microfluxgate and Current Transformer Sensor," IEEE Transactions on Magnetics, August 2022, 10.1109/TMAG.2022.3157052.
[16] C. Lei, Y. Liu, X.-C. Sun, T. Wang, Z. Yang, and Y. Zhou, "Improved Performance of Integrated Solenoid Fluxgate Sensor Chip Using a Bilayer Co-Based Ribbon Core," IEEE Sensors Journal, 15(9):5010–5014, September 2015, 10.1109/JSEN.2015.2432457.
[17] J.-T. Jeng, C.-C. Lu, H.-W. Ku, B.-R. Huang, M.-H. Chia, and X. T. Trinh, "Three-Axis Micofluxgate With a Fluxguide," IEEE Transactions on Magnetics, 55(7):1–4, July 2019, 10.1109/TMAG.2019.2903107.
[18] W.-Y. Choi, J.-S. Hwang, and S.-O. Choi, "The microfluxgate magnetic sensor having closed magnetic path," IEEE Sensors Journal, 4(6):768–771, December 2004, 10.1109/JSEN.2004.836851.
[19] E. Monteblanco, A. Solignac, C. Chopin, J. Moulin, P. Belliot, N. Belin, P. Campiglio, C. Fermon, and M. Pannetier-Lecoeur, "Normalization and Correction Factors for Magnetic Tunnel Junction Sensor Performances Comparison," IEEE Sensors Journal, vol. 21, no. 14, July 2021, 10.1109/JSEN.2021.3076276.

Hugo Nicolas received the B.S. degree in electronics and M.S. degree in microelectronics from the University of Strasbourg, France in 2019 and 2021 respectively. He is currently pursuing the Ph.D. degree at the University of Strasbourg, France, and the University of Applied Sciences, Muttenz, Switzerland since September 2021. His research focuses on the development of a new generation of magnetic sensors using spin transfer torque magnetic tunnel junctions.

Ricardo Sousa received his M.S. degree in Engineering Physics in 1995 from the University of Lisbon and Ph.D. degree in Applied Physics from the Instituto Superior Técnico in Lisbon, for his work on MRAM based on spin dependent magnetic tunnel junctions. He has been working on Magnetic Tunnel Junctions and MRAM at Spintec since 2002, leading the MRAM group there since 2007. He is co-author of 3 book chapters, more than 130 articles, and 16 patents. His research interests are in the field of Spintronic applications, developing sensors and MRAM concepts based perpendicular magnetic anisotropy written by spin transfer torque and all optical switching methods. For his research in thermally assisted MRAM switching, he was a European Descartes Prize finalist in 2006.

Ariam Mora-Hernández received the B.S. degree in physics from University of Veracruz, Mexico in 2012, M.S. degree in theoretical physics from the Center for Research and Advanced Studies of the National Polytechnic Institute, Mexico in 2015 and Ph.D. in Experimental physics at Durham University, United Kingdom in 2020. Since 2021, he is a postdoctoral researcher at the Spintec (CEA), France. His research focuses on nanomagnetism, material physics, interfacial phenomena in thin films and fabrication of MTJs for sensor applications.

Lucian Prejbeanu holds a Ph.D. in Physics from the University of Strasbourg (2001). Senior Member IEEE, he is the executive director of Spintec research laboratory in Grenoble. He is an expert in the field of nanomagnetism and spintronics for magnetic memories and sensors. After his Ph.D., Dr. Prejbeanu joined Spintec, where he pioneered scientific work on thermally assisted MRAM. Based on this proof-of-principle, he was awarded the European Descartes Prize for Research in 2006. Dr. Prejbeanu participated in the creation of the start-up company Crocus Technology. As R&D Director of Crocus, Dr. Prejbeanu led the technological transfer and received in 2012 the joint SEE-IEEE Brillouin prize. Dr. Prejbeanu has authored more than 100 scientific publications and book chapters and is inventor of 46 patents. He is coordinator of the memory pillar of Spintronic Factory, a European network founded in 2016, co-director of the Upstream Technological Platform PTA, one of main nanofabrication centers of RENATECH, French academic network of nanofabrication technology centers and member of the Advisory Committee of IEEE Magnetics.

Luc Hebrard received in 1990 the Engineer and master's degrees in Microelectronics from Ecole Centrale de Lyon (France), and the Ph.D. degree in Microelectronics from ECL in 1993. He held a post-doctoral position at the CNM in Barcelona (Spain) from 1994 to 1995 and was appointed Associate Professor at the University of Strasbourg (Unistra, France) in 1995. From 2004 to 2005, he was a visiting researcher in the Electronic Instrumentation Laboratory at the Technical University of Delft (The Netherlands). He received in 2005 the Accreditation for Research Supervision degree from Unistra and was appointed Full professor at Unistra in 2006. He is with the ICube laboratory and works in the field of integrated instrumentation and its applications, as well as in the field of sensors modeling, and development of specific CAD tools for the design of integrated systems. He was the coordinator of 3 research projects funded by the French Agency of Research (ANR), and scientific head in ten other research projects from ANR or industry. He is a co-author of 110 papers in international conferences and journals. He is a member of the IEEE society. He is involved in several program committees of international conferences and is a member of the steering committee of IEEE NEWCAS.

Jean-Baptiste Kammerer received the Ph.D. degree in microelectronics from the University Louis Pasteur, Strasbourg, France, in 2004. He is currently with the ICube Laboratory, University of Strasbourg, as an Associate Professor. His research interests include integrated sensors, low-noise circuits design, systems and devices' modeling, and heterogeneous systems' design.

Joris Pascal received in 2005 the Engineer and master's degrees in electrical engineering from Ecole Centrale Supélec (France), and the Ph.D. degree in Microelectronics from the University of Strasbourg (France), in 2008. He held scientist and senior scientist positions at ABB Switzerland, Corporate research in Baden-Dättwil (Switzerland) from 2009 to 2015 and was appointed Full Professor at the University of Applied Sciences and Arts Northwestern Switzerland, School of Life Sciences (Switzerland) in 2015. He is at the Institute of Medical Engineering and Medical Informatics and leads the Sensors and Electronics laboratory. He works in the field of instrumentation and its applications in biomedical engineering. He has developed the first Vertical Hall Device in standard CMOS technology, as well as several self-calibrated current and voltage sensors. He was a scientific head in eight other research projects from SNF, SNI, Innosuisse or industry. He is the co-author of 51 papers in international conferences and journals and the inventor of nine patents. He is a member of the Swiss Nanoscience Institute (SNI) and of the IEEE Society.